Chapter 2.2

MECHANICAL PROPERTIES AND DAMAGE DIAGNOSIS OF NATURAL BUILDING STONES

Euripides Papamichos[1], Stefanos-Aldo Papanicolopulos[2] and Idar Larsen[3]
[1]*Aristotle Univ. of Thessaloniki, Dept. of Civil Engineering, GR-54124 Thessaloniki, Greece, epapamic@civil.auth.gr;* [2]*National Technical University of Athens, Dept. of Applied Mathematical and Physical Sciences, GR-15773 Athens, Greece, stefanos@mechan.ntua.gr;* [3]*SINTEF Petroleum Research, N-7465 Trondheim, Norway, idar.larsen@iku.sintef.no*

Abstract: The indentation technique is tailored here to the needs of a portable tool for in situ diagnosis of mechanical properties and damage of natural building stones. Indentation tests were performed in twelve natural building stones (calcarenites, limestones, sandstones, marbles) and mortars used for restoration. A wide range of mechanical and petrophysical properties with different failure mechanisms in indentation is thus represented. Indicatively, the Unconfined Compressive Strength (*UCS*) ranges between 3.1 MPa and 116 MPa and the tangent Young's modulus E_{50} at 50% of the maximum stress in uniaxial compression ranges between 0.9 GPa and 50 GPa. The tests were performed with three indenter diameters, 1-, 2- and 3-mm, to analyze scale effects in the results, and at five different depths, as the technique will be used not only for surface measurements but also for measurements in the interior, at the bottom of a small drilled hole. Such measurements can provide information on stone damage with depth. The results are used to build correlation functions and databases between indentation parameters and stone stiffness and strength. The technique is applied to two marbles that had been artificially weathered with exposure to moisture and temperature cycles, and to a consolidated mortar, i.e. a mortar treated with a consolidant for improving its weathering characteristics.

Key words: indentation test; modulus of flat indentation; critical transition stress; natural building stones; characterization of mechanical properties; damage diagnosis.

1. INTRODUCTION

Stone monuments represent a significant part of our cultural and historical heritage. However, damage (weathering) of historical buildings, monuments, works of art and other cultural properties due to the aggressive urban environ-

S.K. Kourkoulis (ed.), Fracture and Failure of Natural Building Stones, 71–92.

ment of the last decades and the ambient climatic conditions, is reported from all over the world. This has resulted in a substantial effort from local and governmental authorities and the industry for quick and suitable measures for the preservation of national monuments. Several fundamental questions arise in the decision making of the optimum restoration and preservation strategy of old monumental building stones. Among others, there are questions on stone suitability, effectiveness of consolidation measures, and in situ quantitative measurements of the degree of damage of a part or element of a monument or building. Weathering of natural building stones is also of considerable practical interest to the quarrying and the construction industries.

An effort has therefore been undertaken to develop a portable tool that has been missing from the industry for the in situ, quasi non-destructive, reliable and accurate diagnosis of mechanical properties and damage of natural building stones in structures of cultural heritage, in order to improve preservation strategies.

The work builds on previous work by the authors and others on the determination of mechanical properties and damage through indentation testing. The indentation technique is a common method for measuring hardness in metals, glass and ceramics; also for measuring the elastic parameters of surface coatings[1-3]. In rocks, emphasis has been placed in the search for correlations between indentation measurements and rock parameters such as rock strength and stiffness[4-9]. For our purpose the indentation technique is tailored to natural building stone applications.

2. STONE CHARACTERIZATION TESTS

A mechanical and acoustical characterization of 12 common building stones was performed to obtain their basic mechanical and acoustical properties. These properties are used to obtain relations and correlations with the indirect measurements of mechanical properties from indentation tests. They are obtained from conventional triaxial compression tests with acoustics, i.e. ultrasonic wave transmission measurements, and comprise strength, stiffness and dilation parameters, and P- and S- wave velocities. The bulk density is also calculated from the weight and dimension of the specimens.

The tested stones and their origin are listed in Table 1. They comprise one calcarenite, three limestones, three marbles, two sandstones, one soapstone and two mortars. The mortars Block 1 and Block 2 are prepared as twin blocks and therefore have similar properties. Subsequently Block 2 is treated with a consolidant and characterized again to quantify the effect of the consolidation on the mechanical and acoustical properties. The consolidant was supplied by CNR-ICVBC (Italian Research Council, Institute for the Conservation and Promotion of Cultural Heritage) together with the protocol of treatment.

A total of 13 uniaxial, 27 conventional triaxial compression tests each with two load-unload cycles down to almost the confining stress (to capture the elastic behavior), and 13 uniaxial compaction tests were performed. The stones were divided in two groups, the first group of stones 1 to 6 (see Table 1) comprises the weaker stones with $UCS < 50$ MPa and the second group of stones 7 to 12 the stronger stones with $UCS > 50$ MPa. The stones in the first group were tested in triaxial compression at confining stresses of 4 and 10 MPa, while the stones in the second group were tested at confining stresses 5 and 15 MPa.

The main test results are given in Table 1 which lists the grain size, the porosity ϕ, the bulk density ρ, the *UCS*, the static and dynamic Young's moduli E_{50}, E^d_{50} and Poisson's ratios ν_{50}, ν^d_{50} in unconfined tests at 50% of the peak stress, and the peak friction angle φ and peak cohesion c. The peak axial stress in the uniaxial and triaxial tests is plotted in Figure 1 vs. the confining stress.

The marbles are contractant up to or near peak axial stress and show a rather ductile post-peak behavior even at low or zero confining stress. The sandstones are dilatant after about 70% of the peak axial stress and show a rather brittle post-peak behavior. The calcarenite and Pietra di Lecce limestone exhibit pore collapse due to compaction, the Pietra di Vicenza limestone a brittle to ductile behavior with increasing confining stress and the Portland limestone a brittle behavior. The mortars are ductile. With increasing axial stress, the tangent Young's moduli increase and then decrease as the peak stress is approached. In the post-peak region the modulus becomes negative. The tangent Poisson's ratios increase with increasing stress.

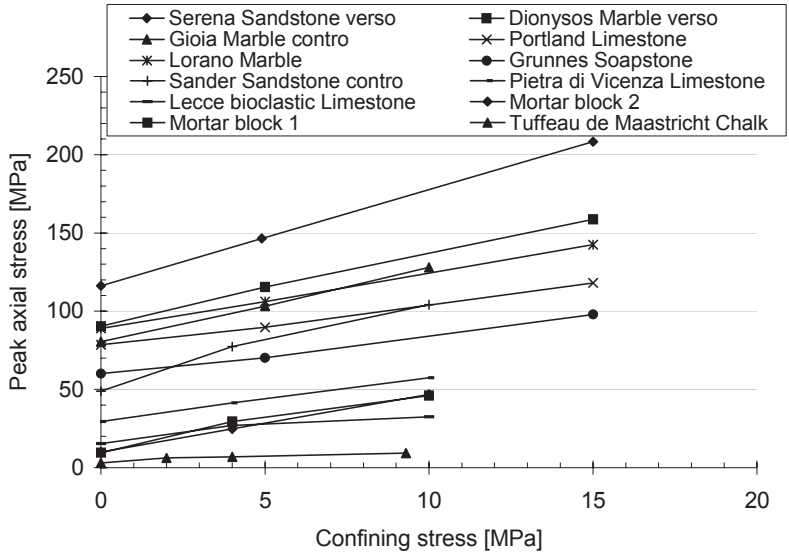

Figure 1. Peak axial stress vs. confining stress in triaxial tests.

Table 1. Stones characterized for their mechanical and acoustical properties

Stone	Origin	Grain size [μm]	ϕ [%]	ρ [g/cm^3]	UCS [MPa]	E_{50} [GPa]	ν_{50} [-]	E^d_{50} GPa]	ν^d_{50} [-]	φ [°]	c [MPa]	K_oS *[MPa]*	M_{50} *[GPa]*	K_{o50} [-]
1. Tuffeau de Maastricht Calcarenite	Netherlands	100	50.0	1.304	3.1	0.90	0.09	3.6	0.14	13.3	1.23	8.0	-	-
2a. Mortar Block 1	Italy	1500	33.0	1.735	9.6	3.8	0.27	8.4	0.24	34.2	3.10	-	1.1	0.8
2b. Mortar Block 2	Italy	1500	33.0	1.742	10.0	3.6	0.15	-	-	34.9	2.62	-	-	-
3. Mortar Block 2 consolidated	Italy	1500	-	1.758	6.2	1.7	0.09	-	-	34.7	1.88	-	-	-
4. Pietra di Lecce Limestone	Italy	80-100	47.4	1.470	15.4	4.8	0.23	10.0	0.23	14.2	6.71	29.6	5.2	0.19
5. Pietra di Vicenza Limestone	Italy	400-2000	29.3	1.948	29.5	15.8	0.31	20.2	0.25	28.1	8.93	67.3	15.3	0.15
6. Sander Sandstone	Germany	150-200	19.7	2.195	48.8	8.8	0.36	23.6	0.23	43.6	11.0	-	10.6	0.32
7. Grunnes Soapstone	Norway	800-2000	0.8	2.895	60.1	29.8	0.39	-	-	25.9	18.5	-	44.4	0.27
8. Portland Island Limestone	UK	300	20.1	2.231	78.5	33.1	0.24	41.9	0.27	27.1	23.8	160.3	33.0	0.16
9. Gioia Marble	Carrara, Italy	150-250	1.5	2.708	80.5	42.1	0.42	53.8	0.32	40.7	18.4	-	47.8	0.24
10. Lorano Marble	Carrara, Italy	-	-	2.710	89.0	49.8	0.25	79.9	0.28	34.3	23.4	-	86.0	0.17
11. Dionysos Marble	Athens, Greece	300-400	1.6	2.708	90.3	45.6	0.32	67.0	0.25	39.7	21.5	-	-	
12. Serena Sandstone	Firenzuola, Italy	200-800	6.5	2.588	116.3	22.7	0.30	43.1	0.22	46.0	23.5	-	27.0	0.23

Generally, the P- and S-wave velocities do not change dramatically with increasing axial stress or during the load-unload cycles. A decrease in the velocities was only observed close and after the peak axial stress demonstrating the damage of the stone. Cycles at axial stress close to the peak stress showed that the decrease in velocity and thus the damage is permanent. The dynamic Young's modulus is generally higher than the static but in the more competent stones it coincides well with the static modulus at the start of the unloading cycles. The dynamic and static Poisson's ratios show generally a reasonable agreement.

In addition, Table 1 lists also the main results from the uniaxial compaction tests, i.e. the uniaxial compaction strength K_oS, and the compaction modulus M_{50} and the K_{o50} value at 50% of the peak axial stress in uniaxial compaction. K_o is the ratio of radial to axial stress in the uniaxial compaction test. From the tested stones, compaction failure experienced the Tuffeau de Maastricht calcarenite and the Pietra di Lecce and Pietra di Vicenza limestones. Shear failure experienced the Portland limestone, while the mortar showed a transition to increased compaction. The remaining stones did not show compaction failure in the range of stresses tested.

3. INDENTATION TESTS

3.1 Test description and program

In the indentation test a normal to the specimen force is applied to an indenter, which penetrates into the specimen under constant displacement (or penetration) rate. Figure 2 shows a schematic view and a photograph of the indentation test equipment, which is placed inside a load frame for the application of the load, test control and data acquisition. A load cell and a Linear Variable Differential Transformer (LVDT) measure, respectively, the applied force and the indentation depth. All tests are performed on oven-dried specimens.

Various indenter shapes, such as flat, hemispherical or conical, and various indenter diameters can be used. Measurements with hemispherical or conical indenters are more difficult to interpret because the contact area varies continuously with indentation depth. With respect to indenter diameter, larger indenters provide more reliable results as they are less affected by the stone's grain size and other inhomogeneities in the petrophysical structure of the stones. However, for high indentation strength stones, the diameter of the indenter may be constrained by the load capacity of the equipment (especially for portable equipment), or the yield or buckling load of the indenter, which can lead to indenter failures (Figure 3a). Based on these, flat indenters with diameters 1-, 2- and 3-mm were used. In this way, an optimum indenter

diameter can be selected according to the stone and indenter properties. The indenter is constructed from hardened at 60 HRC steel with elastic modulus about 190 GPa and yield strength about 2150 MPa at 20ºC. It comprises a 47-mm long and 4-mm diameter stem, a top section for the connection with the load frame holder, and a 2-mm long indentation tip with diameter 1-, 2- or 3-mm (Figure 3b). The stem is necessary in order to perform indentation tests not only at the surface of a stone but also at different depths, i.e. at the bottom of a 5-mm diameter drilled hole. In this way, the mechanical parameters of the stone can be obtained as a function of depth. These parameters in a monumental or other structure may vary due to varying stone degradation.

The indentation tests were performed in stone cubes of 10-cm sides. The vertical orientation of the cubes was selected to coincide with the vertical orientation of the cylindrical specimens tested triaxially for their mechanical

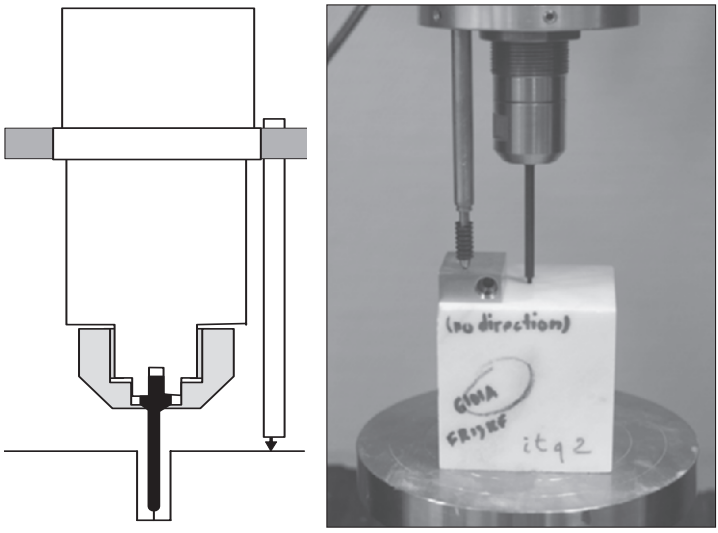

Figure 2. Schematic and photograph of the indentation equipment.

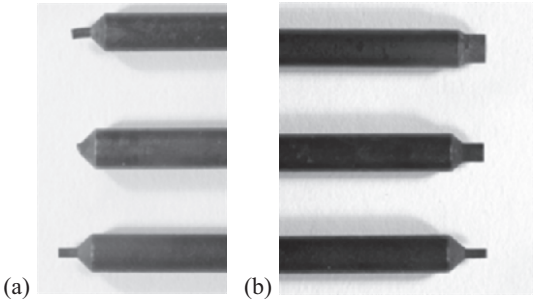

Figure 3. (a) Indenter failures, and (b) indenters with diameter (from top) 3-mm, 2-mm, 1-mm used in testing.

characterization. In each cube, tests were performed with the 1-, 2- and 3-mm indenter in three different locations in a triangular pattern that maximizes the distance between the indenter locations and the corners of the cube to avoid undesirable interaction effects (Figure 4). In each of the three locations, tests were performed at six different depths, i.e. 0-, 5-, 10-, 20-, 30- and 40-mm depths. Finally, the tests were repeated in two more cubes for each stone, cut from the same block. In this way for each of the twelve stones there were three tests for each indenter size and depth, a total of 12×3×3×6=648 tests. Prior to testing and after testing each block, indentation tests were performed in a reference Plexiglas block in order to follow the wear of the indenters in each stone and replace the indenters accordingly. The tests were performed to a maximum indentation depth of 1.5 mm or to a maximum force of 2-, 6- and 9-kN for indenter diameters 1-, 2- and 3-mm, respectively. The indentation rate was about 0.01 mm/s, uncorrected for the indenter deformation.

Figure 5 shows typical test results where the force on the indenter is plotted against the indentation depth for Sander sandstone and Dionysos marble. Generally, the force vs. indentation depth curves show an initial part of increasing slope, a rather linear part and a third part of decreasing slope that may or may not include a peak force. A peak was observed in the marbles, the soapstone and the Serena sandstone, which possibly results from the extensive stone failure around the indenter as shown in Figure 6.

The repeatability of the results is generally satisfactory in the more homogeneous stones but deteriorates as the inhomogeneity increases. Typical example of inhomogeneous material, at least for the scale considered here, is the mortar where different results are obtained when the indentation is performed in a piece of gravel or in the cement (Figure 7).

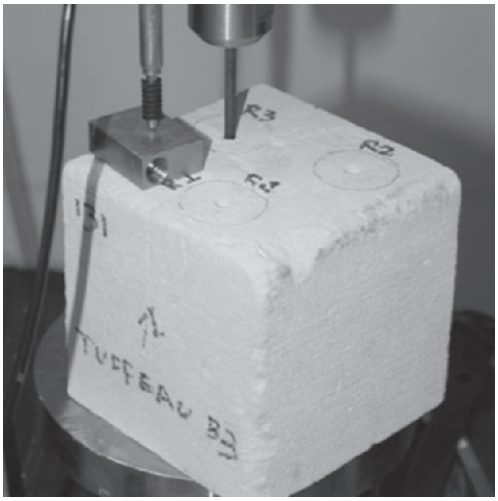

Figure 4. Indentation pattern in a stone block.

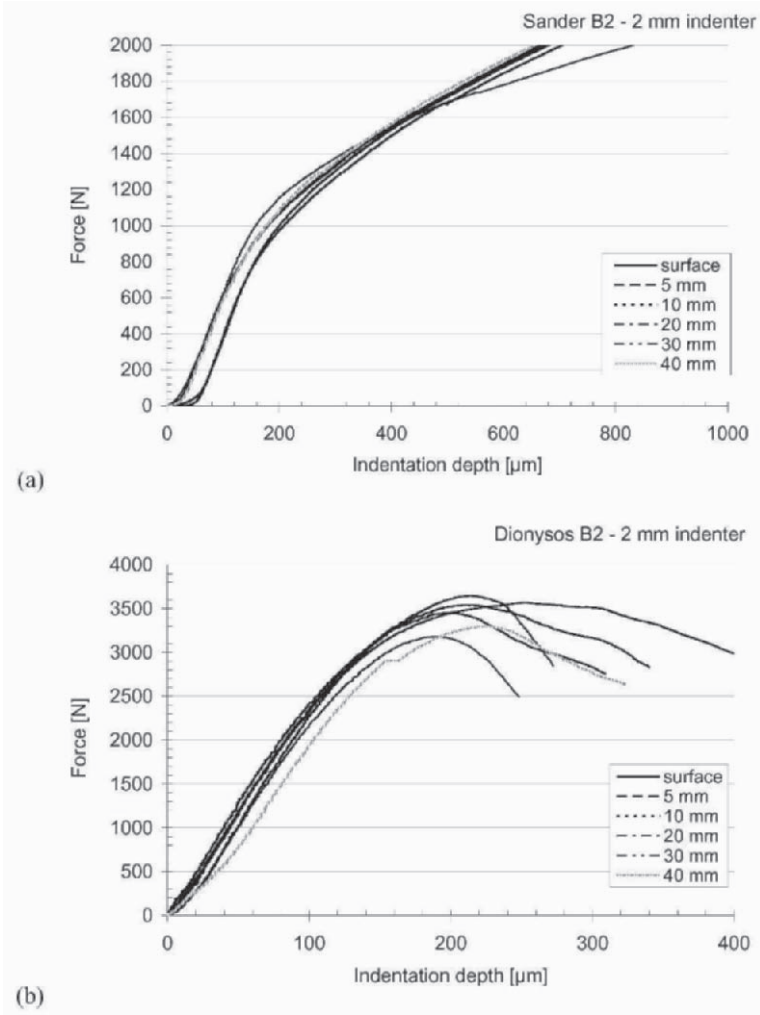

Figure 5. Typical indentation results. Force vs. indentation depth for (a) Sander sandstone and (b) Dionysos marble with 2-mm diameter indenter. Indentations at surface and at five depths.

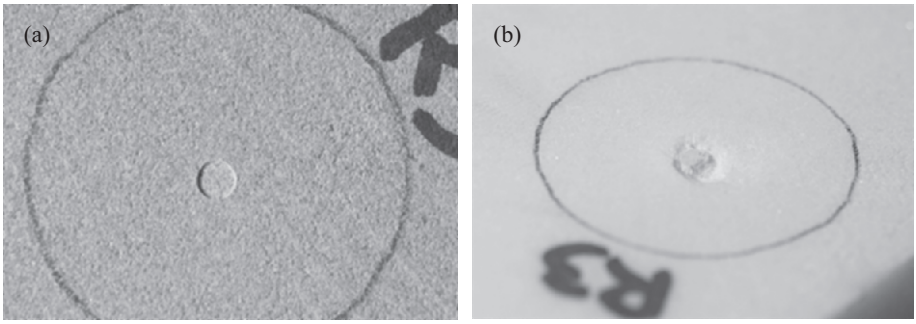

Figure 6. Indentation signature in (a) Sander sandstone and (b) Dionysos marble.

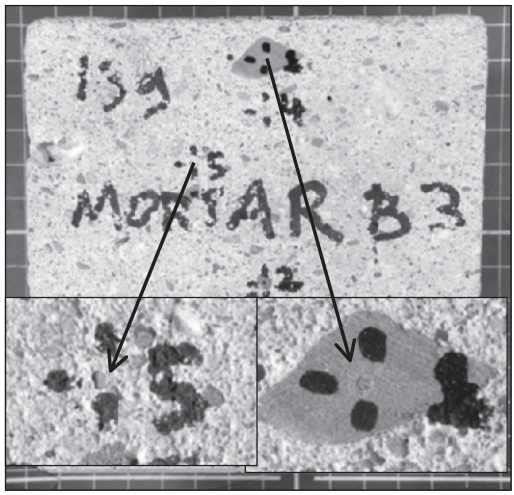

Figure 7. Indentation tests in mortar. Effect of material inhomogeneity on indentation.

3.2 Analysis of indentation results

The results are first corrected for the indenter deformation as a function of force. This is calculated from the indenter's dimensions and elastic modulus. From the corrected results two parameters are calculated, the Scaled Modulus of Flat Indentation and the Critical Transition Stress.

3.2.1 Scaled Modulus of Flat Indentation (*MFIS*)

The Scaled Modulus of Flat Indentation (*MFIS*) with dimensions of stress [Pa], is obtained by scaling the Modulus of Flat Indentation (*MFI*) with the indenter diameter d_i. *MFI* is defined as the slope of the force F vs. indentation depth w curve, at the linear or quasi-linear part of the curve, as shown in Figure 8. The method for calculating *MFI* is to choose first the point in the indentation data where the linear region starts and then finding the linear fit. In cases with particularly noisy data, it is practical to extend the linear region from the best fit until a tolerance in the error function is reached. The slope of this region gives the *MFI*. Alternatively, *MFI* can be calculated from the slope of the region around the inflection point of the curve. This method usually gives a similar *MFI* as the linear region method. However, it was found to be more sensitive to noise in the data or inhomogeneities in the material.

The elastic solution for rigid, flat indentation in a semi-infinite, isotropic, homogeneous material with Young's modulus E and Poisson ratio v is[10]

$$F = \frac{Ed_i}{1-\nu^2} w \tag{1}$$

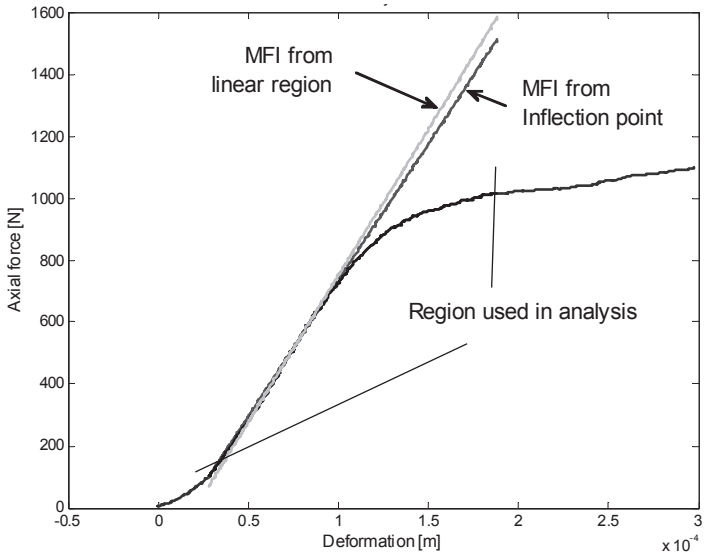

Figure 8. Indentation force vs. indentation depth in a typical indentation test on Dionysos marble. Definition of the region used in the analysis and selection of *MFI* using the linear region method and the inflection point method.

Therefore, according to its definition, the *MFIS* for an isotropic, homogeneous elastic material indented by a rigid, flat indenter is

$$MFIS = \frac{E}{1-\nu^2} \tag{2}$$

and it is independent of the indenter diameter. By extending this expression to inelastic materials, it may be assumed that

$$MFIS \approx \frac{E_{50}}{1-\nu_{50}^2} \tag{3}$$

Therefore, the parameter *MFIS* may be assumed to correlate to E_{50}. The correlations of the calculated values of *MFIS* and the values of E_{50} in uniaxial compression (Table 1) are plotted for each indenter diameter in Figure 9. The results are approximated with power curves of the form

$$E_{50} = b_1 \left(\frac{MFIS}{1\ \text{GPa}} \right)^{b_2} \tag{4}$$

which are also shown in the figure and where the constant b_1 has dimensions of stress [Pa] and the constant b_2 is dimensionless. The values of these constants for the three indenter diameters are given in Table 2 together with the coefficient R^2 of reliability of the approximations. The increase in reliability with indenter diameter shows that small indenters are, as expected,

Table 2. Correlation constants for E_{50} for the 1-, 2- and 3-mm diameter indenters and reliability coefficient R^2

Indenter diameter	Correlation constants b_1 [GPa]	b_2 [-]	Quality of fit R^2 [-]
1-mm	5.0589	0.8014	0.955
2-mm	3.7133	0.7435	0.967
3-mm	3.2639	0.7340	0.988

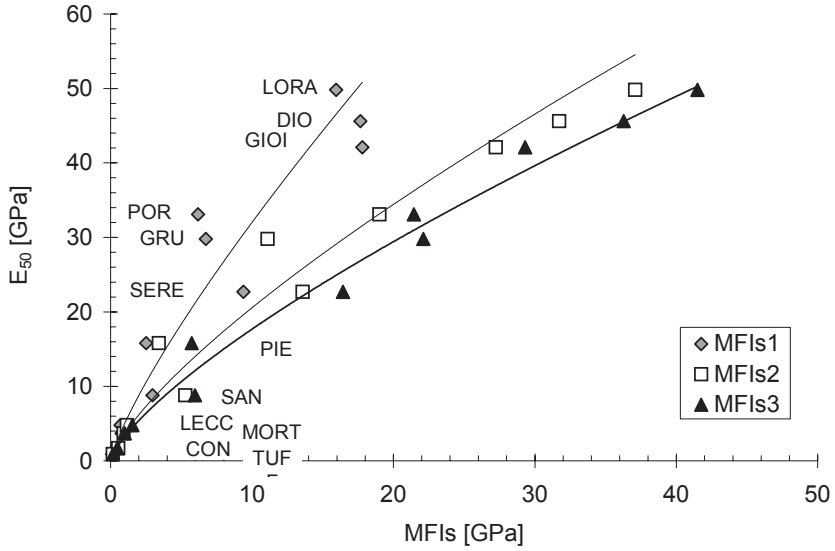

Figure 9. Correlations between uniaxial compression stiffness E_{50} and Scaled Modulus of Flat Indentation *MFIS* for indenter diameter 1-mm (MFIs1), 2-mm (MFIs2) and 3-mm (MFIs3).

more prone to be affected by the internal (petrophysical) structure of the stone. Thus a larger indenter diameter is preferable when the capacity and the specifications of the equipment allow it. The results presented here include data from tests at all depths as the results showed insignificant variations with depth, as it can be seen e.g. in Figure 5.

Reference tests in Plexiglas for indenter diameters 1-, 2- and 3-mm have also shown indenter size-dependency of *MFIS*. For example *MFIS* = 2.79, 3.08 and 3.55 GPa for the 1-mm, 2-mm, and 3-mm indenters, respectively. The indenter size-dependency or scale effect for the tested stones is demonstrated in Figure 10 where the normalized (with the 1-mm indenter diameter values) calibration constants b_{1n} and b_{2n} are plotted vs. the indenter diameter. This size-dependency should be viewed as an average one for all the tested stones whereas individual stones exhibit different size-dependency. A more detail analysis of the size-dependency of *MFIS* for the tested stones is shown in Figure 11, which demonstrates that the *MFIS* is decreasing with decreasing indenter diameter. The size effect varies among the various stones and was measured to be up to approximately 70%.

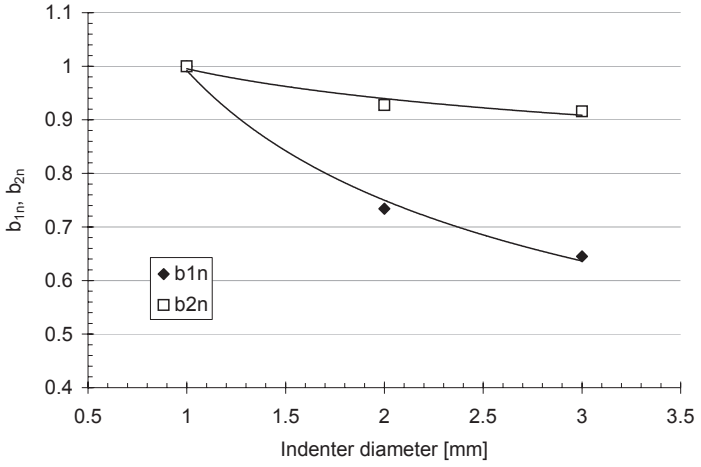

Figure 10. Indenter size-dependency of the calibration constants $b1n$ and $b2n$ for E_{50}.

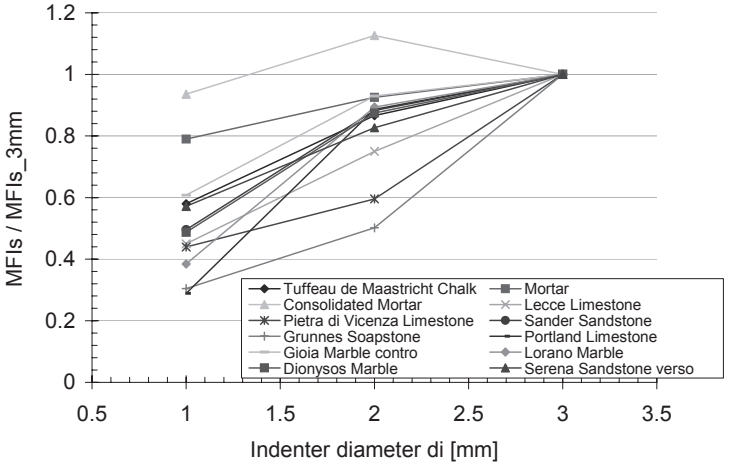

Figure 11. Indenter size-dependency of *MFIS*.

The applicability of Eq.(3) in the indentation of stones may be judged by considering the Elastic Indentation Ratio *EIR* defined as the ratio:

$$EIR = \frac{E_{50}\Big/\left(1-\nu_{50}^2\right)}{MFIS} \tag{5}$$

For an elastic material, this ratio is unity, and thus deviations from unity reflect the degree to which the elastic solution deviates from the test results. For the *MFIS* in Figure 9 and the values of E_{50} and ν_{50} in Table 1, the *EIR*s are plotted in Figure 12 vs. E_{50}. It is noted that, in stones, E_{50} and ν_{50} are not necessarily the elastic parameters but include inelastic effects as well. The re-

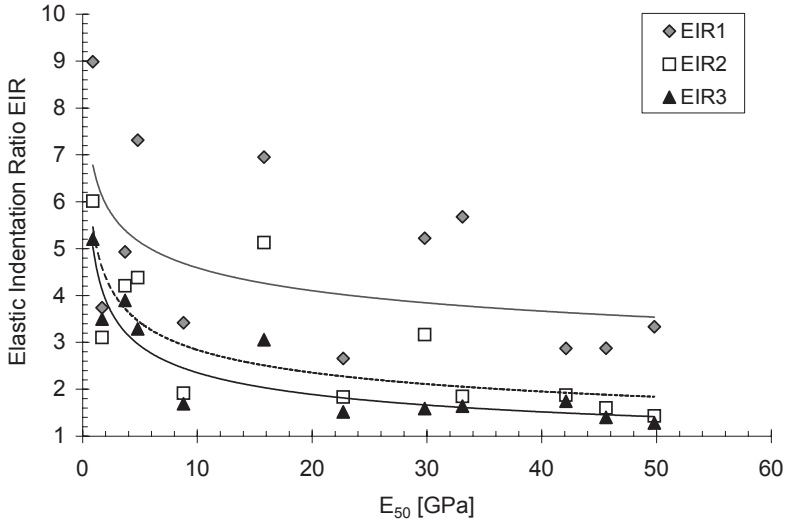

Figure 12. Elastic Indentation Ratio *EIR* vs. E_{50} for indenter diameter 1-mm (EIR1), 2-mm (EIR2) and 3-mm (EIR3).

results show that as the indenter diameter and E_{50} increases, *EIR* approaches unity. This behavior may be interpreted by understanding that with increasing indenter diameter, we move from the softer individual grain and its contacts response to the stiffer response of the stone as a structure. Also the stones with large E_{50} behave more elastically than the low E_{50} stones.

MFIS can also be correlated with the unloading Young's modulus *E*, which can be considered as the elastic Young's modulus of the material since it is calculated from the unloading-reloading cycles of the uniaxial tests. Another correlation can be made with the dynamic Young's moduli E^d_{50} (Table 1), calculated from the P- and S- waves of the uniaxial tests. The correlations for the 3-mm diameter indenter are shown in Figure 13a and are compared with the correlation for the loading Young's modulus E_{50}. All of these correlations show a high fit quality.

Numerical simulations of the flat indentation problem demonstrate that the stress field beneath the indenter is rather one of uniaxial compaction (i.e. zero radial deformation) than one of uniaxial compression (i.e. zero radial stress). Based on this observation it is expected that the indentation stiffness or *MFIS* will correlate well with the uniaxial compaction modulus M_{50} (Table 1), as shown in Figure 13b.

3.2.2 Critical Transition Stress (CTS)

The Critical Transition Stress *CTS*, also with dimensions of stress [Pa], is related to the average stress σ under the indenter, i.e. $\sigma=4F/\pi d_i^2$, at which the force vs. indentation depth curve enters the region of reduced slope. The

material response in this region suggests that some kind of failure takes place. The *CTS* may thus be obtained as the stress at which the slope of the force vs. indenter depth curve differs from the slope that corresponds to *MFIS* with more than a predefined percentage. Alternatively, *CTS* may be calculated from the minimum of the double derivative (or apex) of the force vs. indentation depth in the region of reducing slope (Figure 14).

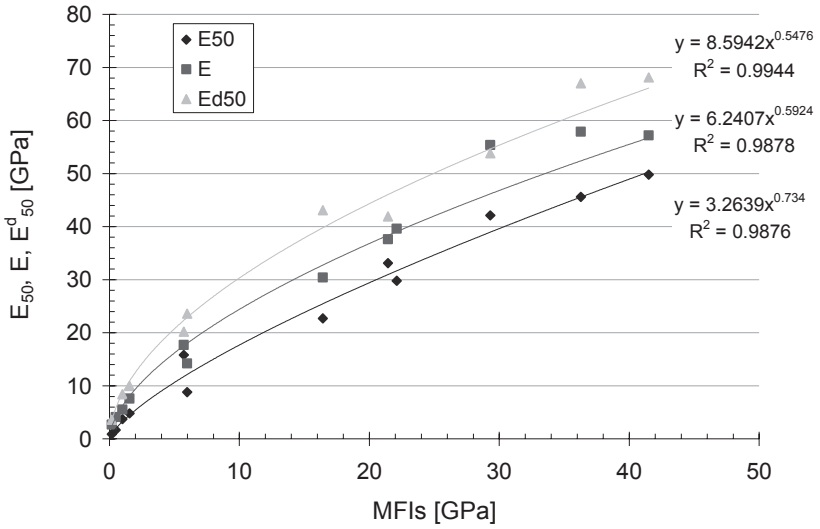

(a)

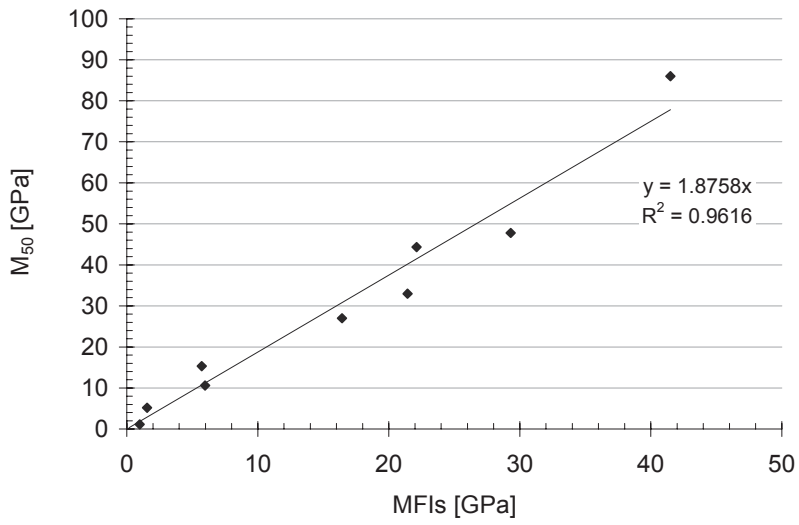

(b)

Figure 13. Correlations between Scaled Modulus of Flat Indentation *MFIS* for 3-mm diameter indenters and (a) uniaxial compression stiffness E_{50}, elastic Young's modulus E, and dynamic Young's modulus E^d_{50}, and (b) uniaxial compaction modulus M_{50}.

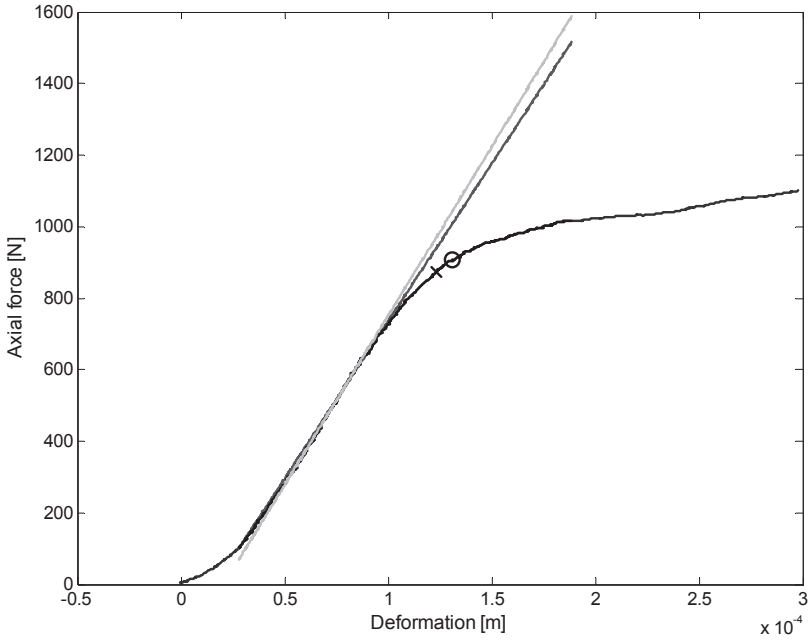

Figure 14. Indentation force versus indentation depth in a typical indentation test on Dionysos marble. The black cross is the *CTS* calculated with a predefined deviation equal to 60% and the black circle is the *CTS* calculated from the curve's minimum of the double derivative.

CTS is correlated with the *UCS* which is a failure strength index in uniaxial compression. This correlation lacks rigorous theoretical background as the stress state in the material under the indenter has a low deviator stress and in reality failure is rather associated with a pressure cap, i.e. grain crushing or pore collapse, than a shear failure surface. This is reflected in the less reliable correlations in Figure 15a between the calculated *CTS* for each indenter diameter and the *UCS* of Table 1. The results are approximated with power curves of the form:

$$UCS = c_1 \left(\frac{CTS}{1\ \text{MPa}} \right)^{c_2} \tag{6}$$

which are also shown in the figure and where the constant c_1 has dimensions of stress [Pa] and the constant c_2 is dimensionless. The values of these constants for the three indenter diameters are given in Table 3 together with the coefficient R^2 of reliability of the approximation.

A failure associated with the pressure cap is encountered in the uniaxial compaction and thus it is expected that the indentation failure stress or *CTS* will correlate with the uniaxial compaction strength K_oS (Table 1), as shown in Figure 15b.

Table 3. Correlation constants for *UCS* for 1-, 2- and 3-mm diameter indenters and reliability coefficient R^2

Indenter diameter	Correlation constants		Quality of fit
	c_1 [MPa]	c_2 [-]	R^2 [-]
1-mm	0.5375	0.7619	0.811
2-mm	0.5098	0.8196	0.8378
3-mm	0.5776	0.8150	0.8526

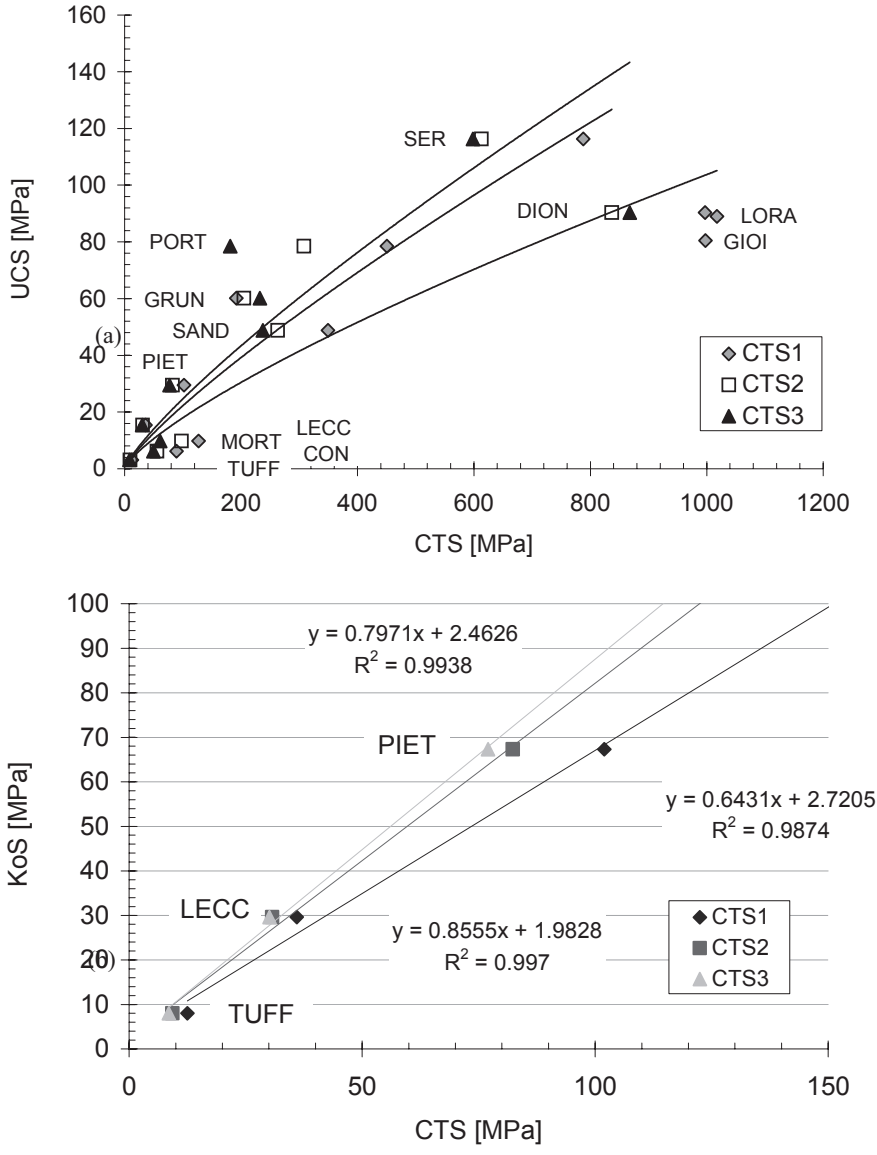

Figure 15. Correlations between (a) *UCS*, and (b) Uniaxial compaction stress K_oS, and Critical Transition Stress *CTS* for indenter diameter 1-mm (CTS1), 2-mm (CTS2) and 3-mm (CTS3).

The data for *CTS* show also an indenter size-dependency for the tested stones. As it is observed in Figure 16, which shows the size dependency of *CTS* for the various stones, this size-dependency is opposite from the size-dependency observed for *MFIS*, i.e. the *CTS* decreases as the indenter diameter increases. Similarly, size-dependency of *CTS* was also observed in Plexiglas for indenter diameters 1-, 2- and 3-mm. For example *CTS*=335.9 MPa for the 1-mm indenter, 299.8 MPa for the 2-mm indenter and 254.7 MPa for the 3-mm indenter.

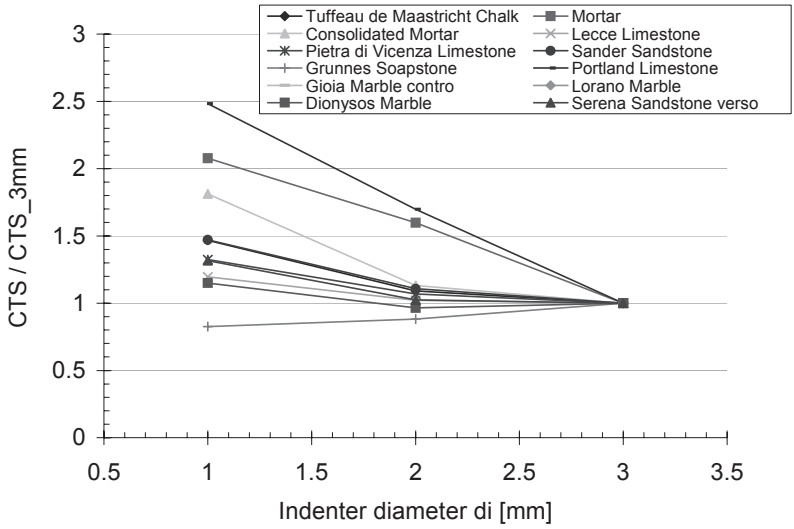

Figure 16. Indenter size-dependency of *CTS*.

4. APPLICATIONS

4.1 Consolidated mortar

The indentation technique was applied for the determination of the effect of a consolidant, as described in Section 2, in the mechanical properties of the mortar. The consolidant was intended to increase the cohesion of monument faces (to a depth of one cm) during restoration works although both triaxial and indentation tests show a deteriorating effect on the mechanical properties and thus it is not appropriate for restoration. From indentation tests with the three indenter diameters and the use of correlations Eqs.(4) and (6), the stiffness E_{50} (in uniaxial compression) and the *UCS* of Mortar and Consolidated Mortar were calculated. These values are compared in Figure 17 with the E_{50} and *UCS* values from uniaxial compression tests (Table 1). The results appear to be satisfactory both quantitatively, i.e. actual values especial-

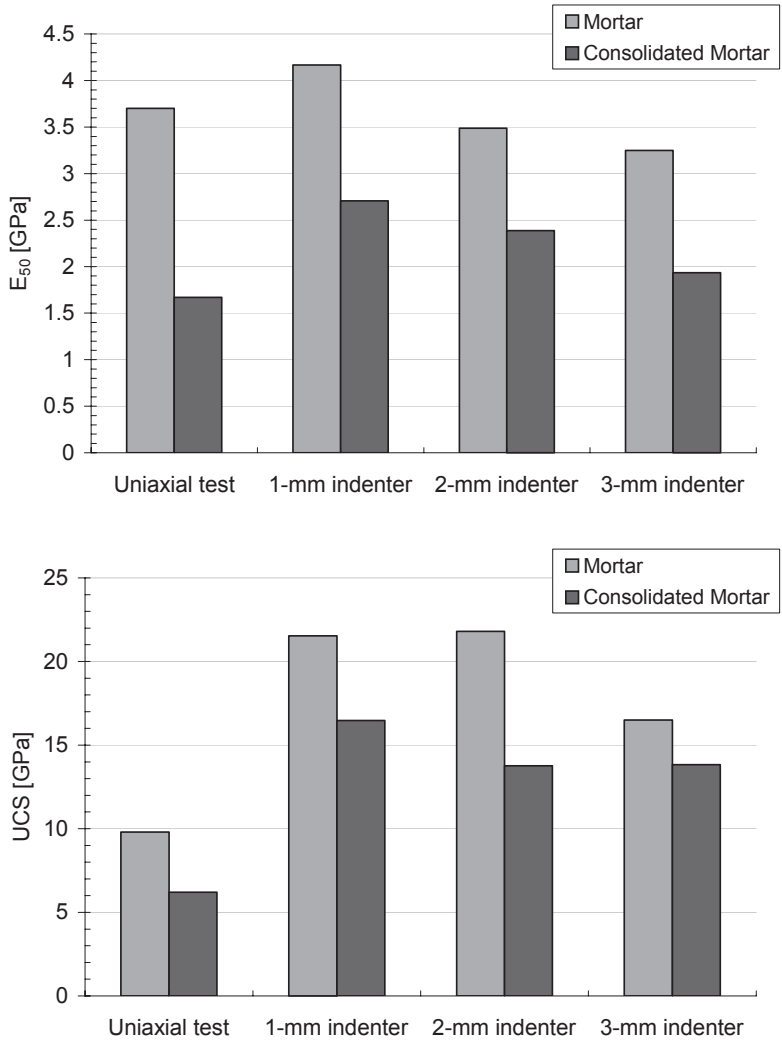

Figure 17. E_{50} (top) and *UCS* (bottom) in Mortar and Consolidated Mortar from uniaxial compression tests and indentation tests with 1-, 2- and 3-mm indenters.

ly for the E_{50}, and qualitatively, i.e. reduction due to consolidant, taken into account the facts that mortar is an inhomogeneous material and in the extreme low of the range of stones tested.

4.2 Artificially-weathered marbles

The indentation technique was also applied for the determination of the effect of artificial weathering of marbles on their mechanical properties. The

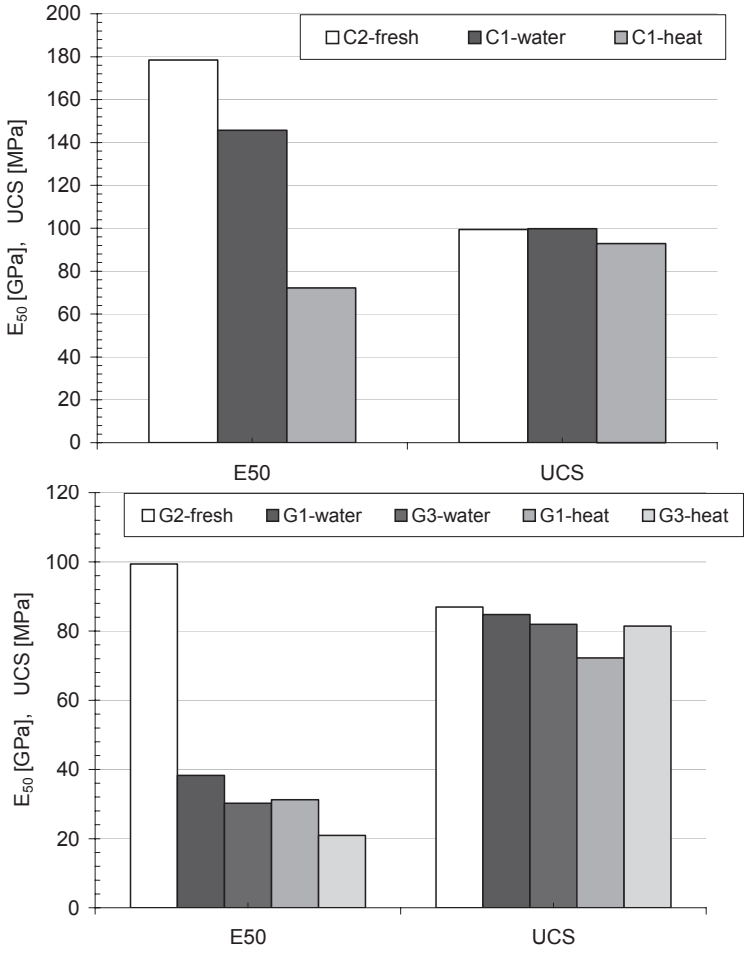

Figure 18. E_{50} and *UCS* in fresh and artificially weathered (heat-treated) Marble 1 (top) and Marble 2 (bottom) from indentation tests.

marbles were weathered using the method NT BUILDT 499 developed to provoke bowing of marbles in an accelerated laboratory environment[11,12]. In this method, a specimen is exposed to water from below and to a number of temperature cycles between 20ºC and 80ºC by heating from above. The specimens are rectangular plates with 30-mm thickness, in accordance with typical panel thickness in claddings. Marble cladding panels are used to cover several modern buildings. At certain buildings the panels start to bow and loose strength after some years. The phenomenon occurs occasionally in crystalline marble exterior claddings[13-14] and is assumed to be controlled by temperature variations and moisture[15].

Twin specimens of two marbles were tested with 1-mm diameter indenters. One of the twin specimens was fresh, i.e. specimens G2 of Marble 1 and C2 of Marble 2, and the others were exposed, i.e. specimens G1 and G3

of Marble 1 and C1 of Marble 2. Of the two marbles, Marble 1 was visibly bowed after exposure while Marble 2 did not show any signs of bowing. On the exposed specimens, both sides, the water- and the heat-side, were indented. From the indentation results and the use of correlations Eqs.(4) and (6), the stiffness E_{50} (in uniaxial compression) and the *UCS* were calculated and plotted in Figure 18. From this figure it is concluded that:

- The degradation effect of moisture and heat cycling is more significant on the stiffness E_{50} than on the *UCS*, and on the heat-side than in the water-side of the specimen.
- Both marbles have suffered degradation of mechanical properties although the degradation appears to be larger in Marble 1, which also was bowed after exposure.
- The E_{50} and *UCS* of fresh Marble 1 (specimen G2) are captured accurately when compared with values in our database.

5. CONCLUSIONS

The indentation technique has been applied for the development of a method for in situ, quasi non-destructive diagnosis of mechanical properties and damage of natural building stones. The method consists of the indentation test specifications, the indentation results analysis, and a correlation database for a wide variety of natural building stones, i.e. calcarenites, limestones, sandstones and marbles, and a mortar used for restoration. From the indentation test data two parameters are calculated, the scaled modulus of flat indentation MFIS and the critical transition stress CTS. From these parameters the following material properties can be derived:

- Tangent stiffness modulus E_{50} in uniaxial compression.
- Elastic Young's modulus E in uniaxial compression.
- Dynamic Young's modulus E^d_{50}.
- Uniaxial compaction stiffness modulus M_{50}.
- Uniaxial compressive strength *UCS*.
- Uniaxial compaction strength K_oS.

where the subscript 50 refers to the value at 50% of the peak axial stress.

The method has been used in the portable and integrated tool DIAS[16], developed for in situ measurements of mechanical properties of natural building stones, both at the surface and at some depth such that the degradation of stone due to weathering can be quantified. The tool is targeted for the preservation and restoration of monuments, although other applications, such as in the construction industry, can benefit from the technique.

The application of the method to a consolidated mortar and two artificially weathered marbles has shown its potential and limitations. The latter are primarily related to the nature of the indentation test, which being a local test is more reliable in homogeneous stones. As an example, the method is not suited for fracture detection in stones. Future work will extend the method to other stone types and especially granites which have not been tested so far.

ACKNOWLEDGEMENTS

The authors acknowledge the support from the EU projects 'Integrated tool for in situ characterization of effectiveness and durability of conservation techniques in historical structures' (DIAS-EVK4-CT-2002-00080) in the framework of the Development of Innovative Conservation Strategies Program, 'Degradation and Instabilities in Geomaterials with Application to Hazard Mitigation' (DIGA-HPRN-CT-2002-00220) in the framework of the Human Potential Program, Research Training Networks, and the project Pythagoras II (EPEAEK II) co-funded by the European Social Fund (75%) and Greek Resources (25%).

REFERENCES

1. B.R. Lawn and R. Wilshaw, Review on indentation fracture: Principles and applications, *J. Material Sci.* **10**, 1049-1081 (1975).
2. R. Mouginot and D. Maugis, Fracture indentation beneath flat and spherical punches, *J. Material Sci.* **20**, 4354-4376 (1985).
3. H.E. Hintermann, Characterization of surface coatings by scratch adhesion test and by indentation measurements, *Fresenius J. Anal. Chem.* **346**, 45-52 (1993).
4. T.W. Miller and J.B. Cheatham, Analysis of the indentation of a compacting material by a perfectly rough wedge, *Int. J. Rock Mech. Min. Sci.* **9**, 475-492 (1964).
5. A.C. van der Vlis, in: *Proc. 2nd Int. Symp. Rock Mech.* (1970), Paper 3-4.
6. J. Geertsma, Some rock mechanical aspects of oil and gas well completions, *SPE J.*, 848-856 (1985).
7. M. Thiercelin and J. Cook, in: *Proc. 29th U.S. Symp. Rock Mech.*, (Balkema, Rotterdam, 1988), pp. 135-142.
8. R. Suárez-Rivera, Z. Zheng, N.G.W. Cook and G. Cooper, in: *Proc. 31st U.S. Symp. Rock Mech.*, (Balkema, Rotterdam, 1990), pp. 671-678.
9. F.J. Santarelli, J.L. Detienne and J.P. Zundel, in: *Proc. 32nd U.S. Symp. Rock Mech.*, (Balkema, Rotterdam, 1991), pp. 647-655.
10. I.N. Sneddon, The relation between load and penetration in the axisymmetric Boussinesq problem for a punch of arbitrary profile, *Int. J. Engng. Sci.* **3**, 47-57 (1965).
11. B. Schouenborg, B. Grelk, J.-A. Brundin and L. Alnæs, Bow test for facade panels of marble, NORDTEST Project 1443-1499 (2000).
12. B. Grelk, P. Golterman, B. Schouenborg, A. Koch and L. Alnæs, in *Proc. Dimension Stone 2004* (2004).

13. J. Cohen and P.J.M. Monteiro, Durability and integrity of marble cladding: A state of the art review, *ASCE Journal* **5**(2), 113-124 (1991).
14. K Hook, Look out below – The Amoco Building cladding failure, *Progressive Architecture* **75**, 58-62 (1994).
15. T. Yates, J.-A. Brundin, P. Goltermann and B. Grelk, in: *Proc..Dimension Stone 2004* (2004).
16. P. Tiano, G. Exadaktylos, E. Papamichos, E. Valentini, in: *Proc. of the HWC-2006 Heritage Weathering and Conservation Conference* (Balkema, Rotterdam, 2006)